Journal of Industrial and Engineering Chemistry 52 (2017) 147–152

Contents lists available at ScienceDirect

Journal of Industrial and Engineering Chemistry

journal homepage: www.elsevier.com/locate/jiec

Surface modification of line-patterned electron transfer layer for enhancing the performance of organic solar cells

Seung E. Jung, Eui J. Lee, Doo K. Moon*, Jung R. Haw*

Department of Materials Chemistry and Engineering, Konkuk University, 120, Neungdong-ro, Gwangjin-gu, Seoul 05029, Republic of Korea

ARTICLE INFO

Article history:
Received 15 December 2016
Received in revised form 15 March 2017
Accepted 22 March 2017
Available online 30 March 2017

Keywords:
Line-pattern
Imprinting
Stamping
Additive
Organic solar cells
Piezoelectric device

ABSTRACT

In this study, we fabricated inverted organic solar cells (i-OSCs) using line-patterned interlayer for electron extraction. The short circuit current density (J_{SC}) of line-patterned interlayer device increased drastically, while the fill factor (FF) decreased rather than flat-type interlayer device. So, an additional flat-type Zinc oxide (ZnO) layer with 1% vol. ethylene glycol (EG) added as an additive between the line-patterned ZnO layer and the ITO electrode was fabricated. The addition of EG in ZnO precursor has reported that the oxygen molecules in EG passivate the surface defects of ZnO and alters its electron affinity of ZnO. As a result, the power conversion efficiency (PCE) of the line-patterned devices introduced an additional flat-type ZnO layer and a ZnO precursor with 1% vol. EG was enhanced from 6.5% to 7.6%.

Introduction

Organic solar cells (OSCs) based on conjugated polymers offer many advantages including low cost, transparency, light weight, and flexibility. They have tremendous attention as next generation renewable power sources for portable and wearable devices such as tablets, laptops, smart watches, and smart phones [1,2]. Several studies have recently been published on OSCs with power conversion efficiencies (PCE) of 10% or more [3]. However, the commercialization potential of OSCs remains questionable, owing to their low efficiency. Hence, a number of studies have been carried out to improve the efficiency of OSCs [4] by using materials with superior photon harvesting [5–7], optimization of phase segregation through additives [8–10], and improving the charge carrier collection through interfacial modifications [2,11,12].

In OSCs, a bulk heterojunction consisting of acceptor and donor polymers is used as the photoactive layer. This layer is positioned between an indium tin oxide (ITO)/poly(3,4-ethylenedioxythiophene:polystyrene sulfonate) (PEDOT:PSS) anode and a low work function metal such as Ba, Al, or Ca [13]. PEDOT:PSS is a transparent electrode material with exceptional electrical and optical properties. However, the acidic and hygroscopic properties of PEDOT:PSS are known to reduce the lifetime of a device [14,15]. This problem can be addressed by using an inverted structure. Kim et al. proposed that the hole collection efficiency of OSCs can be increased by using high work function metals such as Au or Ag and that the device stability can be improved by using air stable metal oxides such as ZnO, TiOx, or ZMO [16].

Among the aforementioned metal oxide candidates for OSCs, ZnO stands out owing to its unique properties such as optical transparency, high electron mobility, and environmental stability. In addition, its solution processability allows an easy morphology control. Owing to its aforementioned characteristics, ZnO is often used as an electron transfer layer (ETL) [13,17,18]. However, calcined ZnO suffers from nanoripples on its surface and charge trapping. This affects the energy band alignment of devices adversely [19]. To eliminate these defects, various methods such as the use of additives or the fabrication of nanostructured ZnO are employed. Poly(ethylene glycol) (PEG) and poly(ethylene oxide) (PEO) are the commonly used additives for controlling the morphology of ZnO. Jo et al. have reported that the addition of PEG to ZnO alters its electron affinity. This is because the oxygen molecules in PEG passivate the surface defects of ZnO, and hence reduce its domain boundaries [20]. Sui et al. and Shao et al. obtained similar results by using PEO as the additive [21,22]. However, their results also showed that as the amount of PEO increases, the performance of OSCs decreases [22].

Fabricating a nanostructure in the buffer layer increases the optical absorption property. As light trapping of an active layer is related to its thickness and morphology, controlling the thickness of the active layer can improve its light absorption property [10].

* Corresponding authors. Fax: +82 2 444 0765.
E-mail addresses: dkmoon@konkuk.ac.kr (D.K. Moon), jrhaw@konkuk.ac.kr (J.R. Haw).

http://dx.doi.org/10.1016/j.jiec.2017.03.037
1226-086X/

Additionally, a functional microprism can be implemented on the top of the glass to further increase the light trapping, which in turn, decreases light scattering [12]. Hu et al. used nanoimprinting lithography on a donor polymer to create numerous devices depending on the pattern size. They found that by decreasing the pattern size, the current density, J_{SC}, can be enhanced since the light absorbance of long-wavelength light increases as the pattern size decreases. However, the Si mold used by them was costly and the process was complicated as the acceptor was thermally evaporated [10]. Jeong et al. and Genevet et al. achieved improved crystallization, chain alignment, and phase separation by implementing nanostructures in photoactive films [2,23].

In the present study, an ordinary digital versatile disc (DVD) was used as the imprinting mold instead of the aforementioned Si mold. To overcome the defects due to imprinting and to enhance the fill factor (FF), a patterned ETL was fabricated on a flat ETL. We used a ZnO ETL since its morphology can be tuned easily, which is favorable for the formation of nanostructures. Ethylene glycol (EG) was added to the flat ETL as an additive for reducing its work function and charge recombination. All this altered the surface electron affinity of the ETL, which in turn, enhanced the energy alignment of the device. As a result, the PCE of the patterned devices increased by approximately 14%.

Experimental section

Preparation of ZnO precursor solution

The ZnO solution was synthesized according to previously published procedures [24]. A gram of zinc acetate dehydrate ($C_4H_6O_4Zn{\cdot}2(H_2O)$ 99.5%, Aldrich) and 0.28 g of monoethanolamine ($HOCH_2CH_2NH_2$, 98%, Aldrich, 1:1 mol ratio) were dissolved into 10 ml of 2-methoxyethanol ($CH_3OC_2H_4OH$, 99.8%, Aldrich) and hydrolyzed for 12 h. The ethylene glycol (EG, $C_2H_4(OH)_2$ 99.8% Aldrich) modified ZnO thin film (ZnO-EG) was prepared by adding 1 vol.% of EG into the 1 ml of ZnO solution.

Preparation of PDMS stamp

To form a nanostructure on ETLs, Polydimethylsiloxane (PDMS) stamp was used. The Shin-Etsu KR-106 and CAT-RG were mixed with a ratio of 10:1 (w/w) [25]. The mixture was stored in vacuum chamber for 30 min to deforming process. After deforming, the mixture was poured on the mold, which was prepared from DVD discs, and annealed at 80 °C for 1 h.

Fabrication of inverted OSCs

To fabricate inverted OSCs, patterned ITO glasses were washed by ultrasonicator with acetone, detergent, 2-propanol and deionized water in sequence. After cleaning, the ITO glasses were baked at 120 °C and UV-ozone-treated for 15 min. The ZnO and ZnO-EG solutions were separately spin-coated onto different ITO glasses and annealed at 150 °C for 1 h in air to obtain an electronic transport layer (ETL, ~10 nm). For the nanostructured devices, after the solutions separately were spin coated on the ITO or ETLs, the PDMS stamp was placed on the surface of the films and pressure of 0.6 MPa was applied on PDMS stamp with 60 °C for 5 min. After imprinting process, the PDMS stamp was peeled off and nanostructured ETLs were annealed at 150 °C for 1 h in air. The prepared samples were then transferred to a N_2-filled glove box, and a solution of polythieno[3,4-b]-thiophene-co-benzodithiophene (PTB7):[6,6]-phenyl C_{71} butyric acid methyl ester ($PC_{71}BM$) (1:1.5, w/w) in chlorobenzene/1,8-diiodooctane (97:3, v/v) was spin-coated to form the photoactive layer (80 nm). Finally, MoO_3 (5 nm) and Ag (100 nm) were sequentially deposited by thermal evaporation in a high-vacuum chamber ($<10^{-7}$ Torr). The active area of the fabricated devices was 12 or 7 mm^2.

Measurement

The current density–voltage (*J–V*) characteristics of the fabricated inverted OSCs were assessed using a Keithley

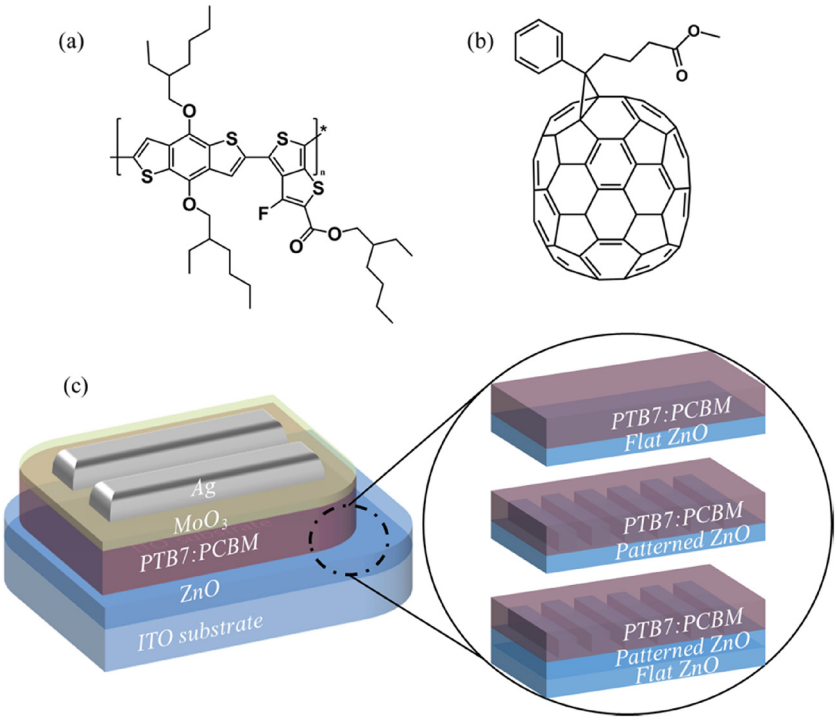

Fig. 1. Molecular structure of (a) PTB7 and (b) $PC_{71}BM$, and (c) device structure of inverted OSCs.

2400 source measure unit and an AM 1.5G solar simulator (Oriel 96000 150 W solar simulator). The incident photon-to-current conversion (IPCE) was measured to determine the best performance of the inverted devices. The surface morphologies and potentials of the ETLs were characterized by AFM and EFM (PSIA XE-100, non-contact mode and external EFM mode). UV–vis spectroscopy (Agilent 8453) was used for changes in light absorption in the devices. And the surface tension was measured using a KRUSS K6 tensionmeter.

Results and discussion

Fig. 1 shows the device structure of the OSC fabricated by us and the molecular structures of PTB7 and $PC_{71}BM$, which were used as the photoactive layers. The inverted structure used for the OSC is shown in Fig. 1(c). A ZnO layer was used as the ETL. ETL structures such as flat-type, line-patterned, double-layered (line-patterned structure on a flat ZnO layer) structures were used. The line-patterned ZnO layer was fabricated by first spin-coating a ZnO precursor on an ITO substrate and then carrying out the imprinting process using a PDMS mold. The double-layer ETL was fabricated by depositing a line-patterned ZnO layer on a flat-type ZnO layer.

The performance of the devices using the flat-type and line-patterned ETLs is shown in Fig. 2 and Table 1. As shown in Fig. 2, the current density of the device using the line-patterned ETL was higher than that of the device using the flat-type ETL. Also, high EQE values are seen over all aspects of IPCE. The PCE of the device with the flat-type ETL was 6.5% (J_{SC} = 13.6 mA/cm^2, V_{OC} = 0.71 V, FF = 66.5%), while that of the device with the line-patterned ETL was 6.6% (J_{SC} = 15.6 mA/cm^2, V_{OC} = 0.69 V, FF = 60.5%) (Table 1). The J_{SC} increased drastically, while the FF decreased as the ETL surface structure changed from flat-type to line-patterned. The results indicate that there was only a slight improvement in the PCE of the devices as the ETL surface structure changed from flat-type to line-patterned.

Fig. 3 shows the UV–vis spectra of the ETL (flat-type and line-patterned structure) deposited on a photoactive layer (glass/ITO/ETL/photoactive). For the device using the line-patterned ETL, the λ_{max} for $PC_{71}BM$ was found to be 375 nm and an improved light absorption was observed over the entire absorption range [10]. The IPCE data shown in Fig. 2(b) showed a similar tendency. The EQE increased in the wavelength range of 300–750 nm. Therefore, the increased J_{SC} value can be explained by the increased light absorption in the photoactive layer, which was obtained by using the line-patterned ETL [26].

Line-patterning of the ZnO structure was done by an imprinting process. The line-patterning of the ETL allowed the scattering of light, which in turn enhanced the light absorption in the photoactive layer formed on the top of the ETL. Furthermore, a plasmonic effect and back scattering of the light incident onto the device was observed in the interface between the photoactive layer and the Ag electrode formed on the top of the ETL by creating a pattern similar to the ETL surface. Consequently, the light trapping properties within the photoactive layer were improved, thereby increasing the J_{SC} of the OSC [3,12,27].

Table 1
Device performance of OSCs.

ETL	Voc [V]	Jsc [mA/cm$_2$]	FF [%]	PCE [%]	R_s [Ωcm^2]
Flat ZnO	0.71 (0.71)	13.6 (13.6)	66.5 (65.3)	6.5 (6.4)	5.2
Patterned ZnO	0.69 (0.69)	15.6 (15.2)	60.5 (59.4)	6.6 (6.5)	7.2

The values in the parentheses present average values of 4 cells.

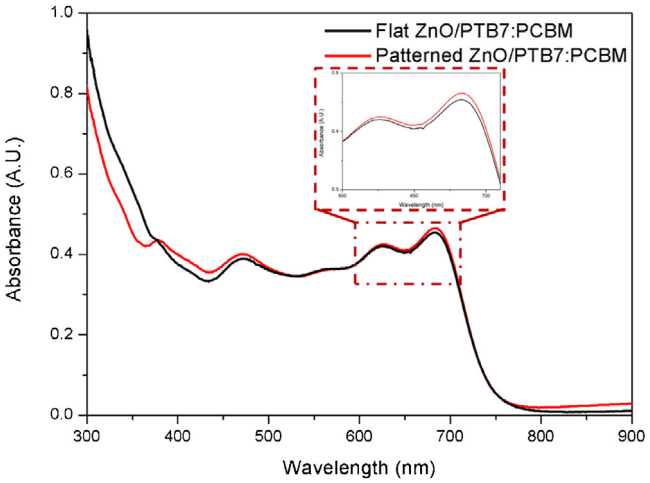

Fig. 3. Light absorbance of photoactive layer with ZnO ETL.

Fig. 4 shows the topology and measured surface potential (SP) of the flat-type and line-patterned ETL surfaces. The flat-type ETL was fabricated by spin coating a ZnO precursor. Fig. 4(a) shows that a nanoripple [28] was formed on the surface of the flat-type ETL. On the other hand, the surface of the line-patterned ZnO layer (Figs. 4(b) and S1 (see Supporting information)) showed periodic nano-patterns formed at the intervals of 700 nm. Fig. 4(c) and (d) shows the SP of the flat-type and line-patterned ZnO layers measured using an EFM, respectively. SP varies significantly with the changes in the electronic states of the surface, which might be caused by the factors such as the surface charge density or surface traps, surface reconstruction, and chemical composition [29]. The mean SP of the line-patterned ZnO layer (37.51 mV) was greater than that of the flat-type ZnO layer. Furthermore, the SP difference between the thickest (peak) and the thinnest (valley) parts of the film (ΔPV) was measured to be 28.68 mV for the line-patterned ZnO layer. This value is significantly greater than the ΔPV measured for the flat-type ZnO

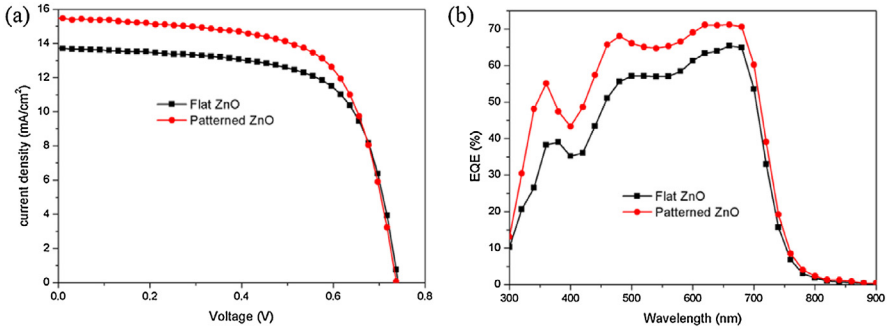

Fig. 2. (a) Current density (J) – voltage (V) characteristics and (b) external quantum efficiency (EQE) characteristics of OSCs.

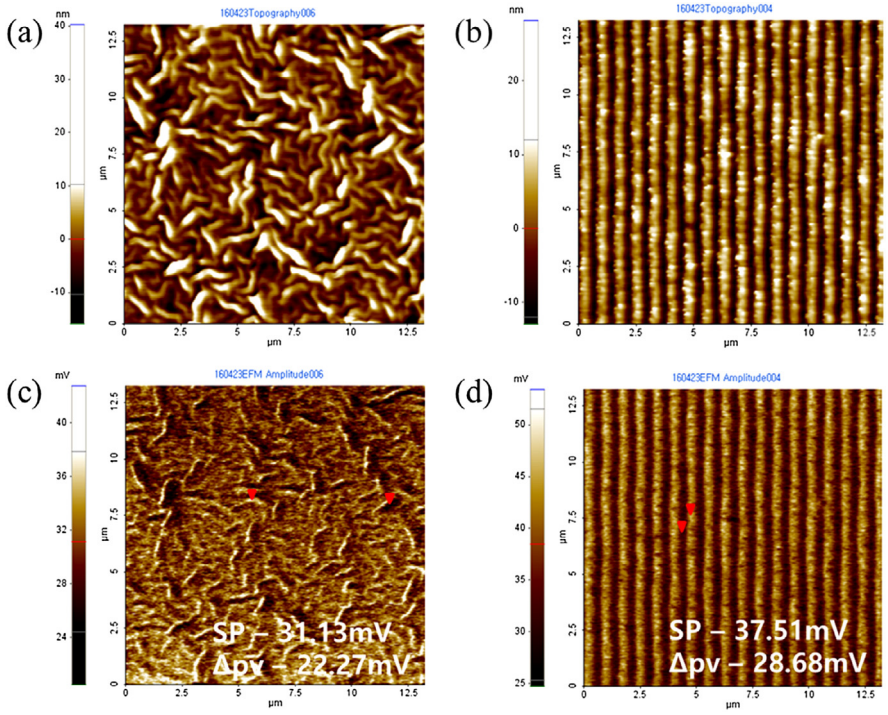

Fig. 4. AFM images of (a) flat ZnO and (b) patterned ZnO and EFM images of (c) flat ZnO and (d) patterned ZnO.

(22.27 mV). The imprinting process resulted in a larger ΔPV on the surface of the line-patterned ZnO layer. When pressure is applied onto a ZnO layer covered with a PDMS mold for line-patterning formation, a line-patterned layer with a height corresponding to the depth of the mold is formed and the remaining portion forms a residual layer [11]. However, in our case, when the ZnO ETL consisted of a single layer, the overall thickness of the ETL was smaller than the depth of the mold. This resulted in the formation of an extremely thin residual layer. In this case, a partial contact might have occurred between the ITO and the photoactive layer, resulting in an increased R_S and a decreased FF [10].

To address the aforementioned problem of FF reduction in the line-patterned ZnO layer, a new device with an additional flat-type ZnO layer between the line-patterned ZnO layer and the ITO electrode was fabricated. We used a pristine ZnO precursor and a ZnO precursor with 1% vol. EG added as an additive to form the flat-type ZnO layer. As can be seen from Fig. S2 and Table S1 (see Supporting information), the optimized device with flat-type EG-ZnO showed higher *Voc* and PCE than flat-type ZnO based device. The performance of the OSCs with this configuration is shown in Fig. 5 and Table 2. It can be observed that the PCE of the device with the pristine precursor-derived flat-type ZnO layer was 7.1% (J_{SC} = 15.3 mA/cm^2, V_{OC} = 0.67 V, *FF* = 68.5%). Compared to the device without the additional flat-type ZnO layer, this device showed a significantly larger FF. Similarly, the device with the EG-modified flat-type-ZnO layer (with a PCE value of 7.6% (J_{SC} = 15.5 mA/cm^2, V_{OC} = 0.73 V, *FF* = 66.1%)) also showed a higher FF as compared to the device without the additional flat-type ZnO layer.

The enhanced performance of the device with the additional flat-type ZnO layer is attributed to the change in the surface properties of the line-patterned ZnO layer. The AFM images and EFM data shown in Fig. 6 show that the ZnO layer in this case had periodic line-patterns similar to those shown in Fig. 4(b). However, ΔPV of the ETL surface was reduced by the additional flat-type ZnO layer, forming an uniform SP on the ETL surface. The flat-type ZnO layer formed below the line-patterned ZnO layer acted as a residual layer, thus decreasing ΔPV of the extremely thin residual ZnO layer, as shown in Fig. 4(d). The increased thickness of the overall residual layer also prevented any contact between the photoactive layer and the ITO electrode, resulting in a reduced R_S and an increased FF.

In the new configuration, the surface properties on the line-patterned ZnO layer were found to be dependent of the flat-type ZnO layer (Figs. 6 and 7). Fig. 7 shows that the modification of

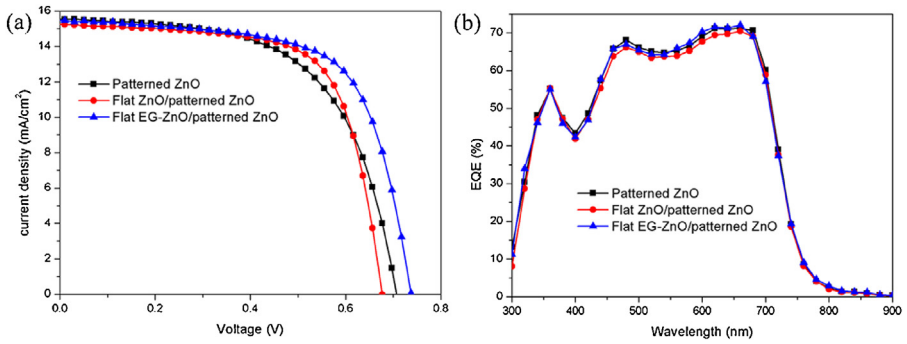

Fig. 5. (a) Current density (*J*) – voltage (*V*) characteristics and (b) external quantum efficiency (EQE) characteristics of OSCs with patterned ZnO ETLs.

Table 2
Device performance of OSCs with patterned ZnO ETLs.

ETL	Voc [V]	Jsc [mA/cm$_2$]	FF [%]	PCE [%]	R_s [Ωcm^2]
Patterned ZnO	0.69 (0.69)	15.6 (15.2)	60.5 (59.4)	6.6 (6.5)	7.2
Flat ZnO/Patterned ZnO	0.67 (0.67)	15.3 (15.2)	68.3 (67.4)	7.1 (6.9)	4.87
Flat EG-ZnO/Patterned ZnO	0.73 (0.73)	15.5 (15.2)	66.1 (66.1)	7.6 (7.3)	5.9

The values in the parentheses present average values of 4 cells.

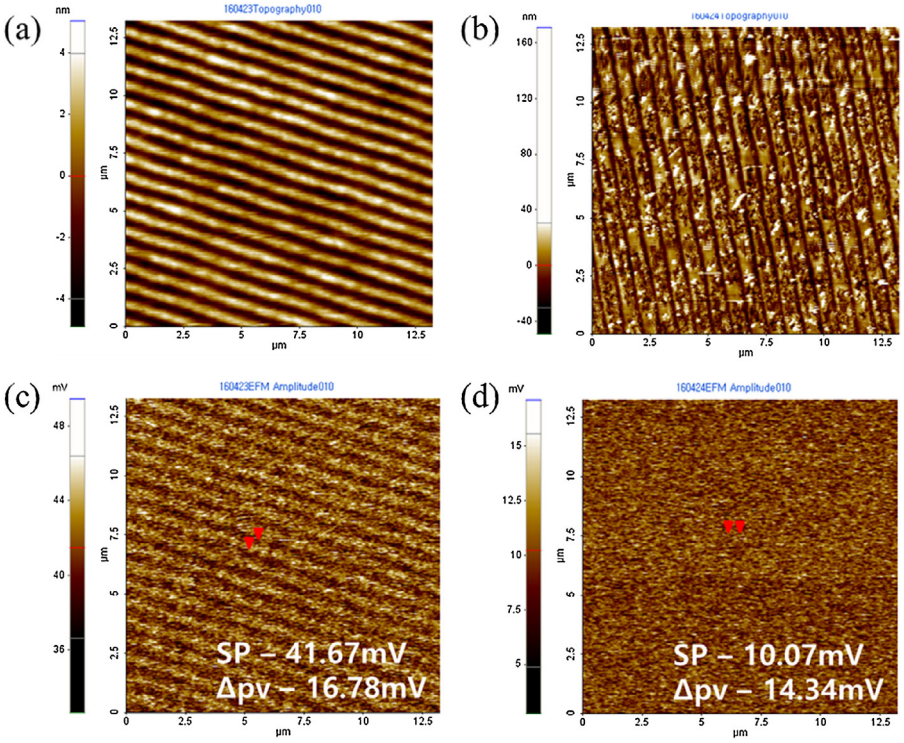

Fig. 6. AFM images of (a) flat ZnO/patterned ZnO and (b) flat EG-ZnO/patterned ZnO and EFM images of (c) flat ZnO/patterned ZnO and (d) flat EG-ZnO/patterned ZnO.

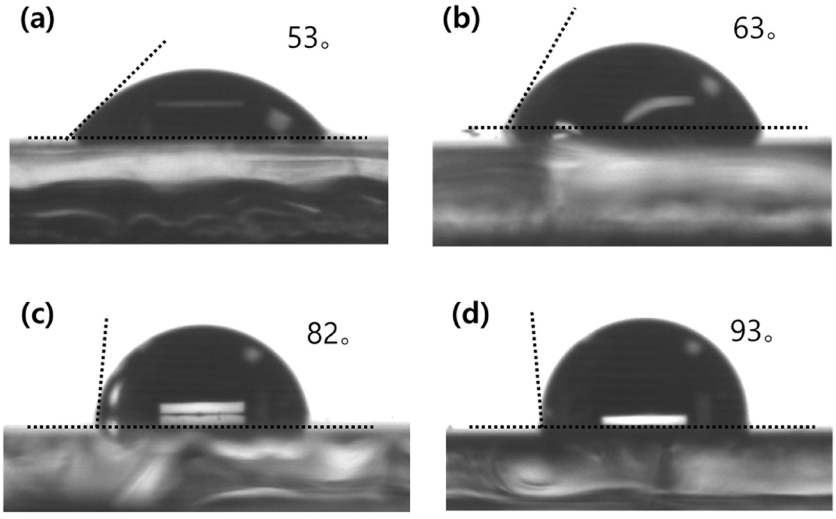

Fig. 7. Contact angle of D.I. water on ETLs; (a) flat ZnO, (b) patterned ZnO, (c) flat ZnO/patterned ZnO and (d) flat EG-ZnO/patterned ZnO.

the ZnO surface structure produced changes in the surface hydrophobicity of the ZnO layer. The increased contact angle of DI water indicates that the ETL surface became more hydrophobic. The increased hydrophobicity of the ETL surface contributed to the structural change of the ZnO surface. This favored the formation of the photoactive layer, which is also hydrophobic, on the ETL surface. The two layers then came in a close contact with each other, resulting in an enhancement of the device

performance [30]. Fig. 6(c) and (d) shows that mean SP decreased significantly to 10.07 mV with the implementation of the EG-modified flat-type ZnO layer. This change in the SP can be explained by the crystallinity of ZnO. The addition of EG, which is the simplest diol, to the ZnO precursor enhanced the crystallinity of ZnO [31] (Fig. S3 of Supporting information). Furthermore, the addition of EG can also modify the morphology of ZnO. Because of the change in the crystallinity of ZnO, the SP of the OSC with new configuration also decreased. As electrons build up on the surface of an ETL, charge trapping can create a band bending in its valence and conduction bands. The bending effect on the valence and conduction bands increased and the ETL work function (WF) decreased as the SP increased [32]. Therefore, the device with the EG-modified flat-type ZnO layer/line-patterned ZnO layer with a relatively low SP lowered the energy barrier between the ETL and the photoactive layer. This is because EG passivates the surface defects on ZnO, resulting in reduced charge trapping. This in turn allows for the tuning of the overall energy level of the device. Thus, it can be concluded that these effects increased the V_{OC} of the device [13].

Conclusion

In this study, we employed a line-structured ETL to enhance the light absorption in the photoactive layer. The SP of the ETL was controlled by adding an extra flat-type ZnO layer between the imprinted ETL and the ITO electrode. Furthermore, using EG as an additive in the flat-type ZnO layer resulted in the modification of the SP of the flat-type ZnO layer/line-patterned ZnO layer. As a result, the optimized OSC device showed a PCE of 7.6%, which is 17% more than that of the device with only the flat-type ETL. This is because the implementation of an additional flat-type ZnO layer and tuning of the surface properties of the flat-type ZnO layer prevented the generation of disordered electric SP.

Associated content

AFM images of imprinting stamp and AFM images of surface topography of as-casted ETLs as concentration of ethylene glycol.

Acknowledgment

This paper was supported by Konkuk University in 2014.

Appendix A. Supplementary data

Supplementary data associated with this article can be found, in the online version, at http://dx.doi.org/10.1016/j.jiec.2017.03.037.

References

[1] J.W. Leem, S. Kim, S.H. Lee, J.A. Rogers, E. Kim, J.S. Yu, Adv. Energy Mater. 4 (8) (2014) 1, doi:http://dx.doi.org/10.1002/aenm.201301315.
[2] S. Jeong, C. Cho, H. Kang, K.-H. Kim, Y. Yuk, J.Y. Park, B.J. Kim, J.-Y. Lee, ACS Nano 9 (3) (2015) 2773, doi:http://dx.doi.org/10.1021/nn506678a.
[3] J.W. Leem, S. Kim, C. Park, E. Kim, J.S. Yu, ACS Appl. Mater. Interfaces 7 (12) (2015) 6706, doi:http://dx.doi.org/10.1021/acsami.5b00101.
[4] Y.S. Cheng, C. Gau, Sol. Energy Mater. Sol. Cells 120 (Part B) (2014) 566, doi:http://dx.doi.org/10.1016/j.solmat.2013.09.040.
[5] C. Soci, I.W. Hwang, D. Moses, Z. Zhu, D. Waller, R. Gaudiana, C.J. Brabec, A.J. Heeger, Adv. Funct. Mater. 17 (4) (2007) 632, doi:http://dx.doi.org/10.1002/adfm.200600199.
[6] M.H. Choi, K.W. Song, D.K. Moon, J.R. Haw, J. Ind. Eng. Chem. 29 (2015) 120, doi:http://dx.doi.org/10.1016/j.jiec.2015.03.024.
[7] M.-H. Choi, E.J. Ko, Y.W. Han, E.J. Lee, D.K. Moon, Polymer (Guildf) 74 (2015) 205, doi:http://dx.doi.org/10.1016/j.polymer.2015.08.003.
[8] S.W. Heo, S.H. Kim, E.J. Lee, D.K. Moon, Sol. Energy Mater. Sol. Cells 111 (0) (2013) 16, doi:http://dx.doi.org/10.1016/j.solmat.2012.12.027.
[9] S.W. Heo, K.W. Song, M.H. Choi, H.S. Oh, D.K. Moon, Sol. Energy Mater. Sol. Cells 114 (2013) 82, doi:http://dx.doi.org/10.1016/j.solmat.2013.02.004.
[10] L. Wang, S. Zhao, Z. Xu, J. Zhao, D. Huang, L. Zhao, Materials (Basel) 9 (3) (2016) 1, doi:http://dx.doi.org/10.3390/ma9030171.
[11] Y. Yang, K. Mielczarek, A. Zakhidov, W. Hu, (2014).
[12] Y.H. Lee, T.K. Lee, I. Song, H. Yu, J. Lee, H. Ko, S.K. Kwak, J.H. Oh, Adv. Mater. 28 (25) (2016) 4976, doi:http://dx.doi.org/10.1002/adma.201506479.
[13] E.J. Lee, S.W. Heo, Y.W. Han, D.K. Moon, J. Mater. Chem. C (2016), doi:http://dx.doi.org/10.1039/C5TC03754A.
[14] M.-H. Choi, E.J. Lee, J.P. Han, D.K. Moon, Sol. Energy Mater. Sol. Cells 155 (2016) 243, doi:http://dx.doi.org/10.1016/j.solmat.2016.06.017.
[15] W. Qiu, R. Müller, E. Voroshazi, B. Conings, R. Carleer, H.-G. Boyen, M. Turbiez, L. Froyen, P. Heremans, A. Hadipour, ACS Appl. Mater. Interfaces 7 (6) (2015) 3581, doi:http://dx.doi.org/10.1021/am507459t.
[16] C.S. Kim, S.S. Lee, E.D. Gomez, J.B. Kim, Y.L. Loo, Appl. Phys. Lett. 94 (11) (2009), doi:http://dx.doi.org/10.1063/1.3099947.
[17] A.K.K. Kyaw, X.W. Sun, C.Y. Jiang, G.Q. Lo, D.W. Zhao, D.L. Kwong, Appl. Phys. Lett. 93 (22) (2008) 1, doi:http://dx.doi.org/10.1063/1.3039076.
[18] T. Hu, F. Li, K. Yuan, Y. Chen, (2013).
[19] O. Pachoumi, A.A. Bakulin, A. Sadhanala, H. Sirringhaus, R.H. Friend, Y. Vaynzof, J. Phys. Chem. C 118 (33) (2014) 18945, doi:http://dx.doi.org/10.1021/jp506266f.
[20] S.B. Jo, J.H. Lee, M. Sim, M. Kim, J.H. Park, Y.S. Choi, Y. Kim, S. Ihn, K. Cho, (2011) 690, doi: 10.1002/aenm.201100154.
[21] X. Sui, C. Shao, Y. Liu, 48 (2007) 1459, doi: 10.1016/j.polymer.2007.01.039.
[22] S. Shao, K. Zheng, T.T. Pullerits, F. Zhang, ACS Appl. Mater. Interfaces 5 (2) (2013) 380, doi:http://dx.doi.org/10.1021/am302408w.
[23] P. Genevet, J. Lin, M. a Kats, F. Capasso, Nat. Commun. 3 (2012) 1278, doi:http://dx.doi.org/10.1038/ncomms2293.
[24] K. Yuan, L. Chen, F. Li, Y. Chen, J. Mater. Chem. C 2 (6) (2014) 1018, doi:http://dx.doi.org/10.1039/C3TC32071E.
[25] K. Efimenko, W.E. Wallace, J. Genzer, J. Colloid Interface Sci. 254 (2) (2002) 306, doi:http://dx.doi.org/10.1006/jcis.2002.8594.
[26] S.H. Liao, H.J. Jhuo, Y.S. Cheng, S.A. Chen, Adv. Mater. 25 (34) (2013) 4766, doi:http://dx.doi.org/10.1002/adma.201301476.
[27] J. Li, S.K. Cushing, P. Zheng, F. Meng, D. Chu, N. Wu, Nat. Commun. 4 (2013) 1, doi:http://dx.doi.org/10.1038/ncomms3651.
[28] H.-Y. Park, D. Lim, K.-D. Kim, S.-Y. Jang, J. Mater. Chem. A 1 (21) (2013) 6327, doi:http://dx.doi.org/10.1039/c3ta10637c.
[29] H. Zhou, Y. Zhang, J. Seifter, S.D. Collins, C. Luo, G.C. Bazan, T.Q. Nguyen, A.J. Heeger, Adv. Mater. 25 (11) (2013) 1646, doi:http://dx.doi.org/10.1002/adma.201204306.
[30] S.W. Heo, E.J. Lee, K.W. Seong, D.K. Moon, Sol. Energy Mater. Sol. Cells 115 (2013) 123.
[31] S. Ashoka, G. Nagaraju, C.N. Tharamani, G.T. Chandrappa, Mater. Lett. 63 (11) (2009) 873, doi:http://dx.doi.org/10.1016/j.matlet.2009.01.054.
[32] J.N. Barisci, R. Stella, G.M. Spinks, G.G. Wallace, Synth. Met. 124 (2–3) (2001) 407, doi:http://dx.doi.org/10.1016/s0379-6779(01)00387-3.